Mechanical sensors

Air-Coupled Whispering Gallery Mode On-Chip Microspherical Shell Resonator for High-Frequency Ultrasound Detection

Chichen Huang, Jiayuan Zhang, and Srinivas Tadigadapa*

Department of Electrical and Computer Engineering, Northeastern University, Boston, MA 02115 USA
**Fellow, IEEE*

Manuscript received 23 June 2024; revised 9 July 2024; accepted 22 July 2024. Date of publication 25 July 2024; date of current version 13 August 2024.

Abstract—In this letter, we report on a high-sensitivity whispering gallery mode (WGM) resonator-based air-coupled ultrasound sensor capable of detecting minute pressure variations across an ultrasound frequency spectrum of 0.6–3.5 MHz. The sensor comprises a microspherical glass shell of approximately 450 μm in radius and nonuniform shell thickness of 7–15 μm, which is optically coupled to a tunable laser for resonance excitation. The setup allows for the precise measurement of acoustic signals, benefiting from the high optical Q-factor of ~2 million of the blown glass microspherical shells. A noise equivalent pressure as low as 40 $\mu\text{Pa}/\sqrt{\text{Hz}}$ was obtained at 1.72-MHz ultrasound frequency. A very good correspondence between the simulated axisymmetric resonance frequencies measured using the WGM resonator and a 3D finite-element analysis model in COMSOL was established. The sensor showed an expected linear dependence on the drive voltage of the ultrasound transducer. The distortion of the microspherical shell under acoustic pressure was also independently confirmed using a laser Doppler vibrometer. The sensor's capability to handle high-frequency ultrasonic waves with significantly better signal-to-noise ratio than conventional piezoelectric- or microphone-based systems is demonstrated, highlighting its suitability for advanced photoacoustic applications.

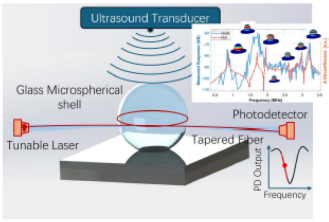

Index Terms—Mechanical sensors, acoustic measurement, microspherical shells, optical sensing, optomechanical systems, ultrasound sensors, whispering gallery mode (WGM) resonators.

I. INTRODUCTION

High-sensitivity ultrasound sensors capable of detecting megahertz range acoustic signals in air are highly desirable. These sensors are specifically motivated by the higher resolution ultrasound imaging needs, particularly crucial in photoacoustic (PA) spectroscopy and in medical settings where the ability to detect subtle changes in tissue structure can significantly impact diagnostic accuracy and outcomes [1], [2]. The large acoustic impedance mismatch at the interface between air and ultrasound transducers requires the use of a medium, such as water or gel, for the effective coupling and transmission of ultrasound [3]. However, in many applications where contact with the medium is impractical or could damage delicate samples, air-coupled ultrasound sensing is essential [4], [5]. In addition to the high coupling losses at air transducer interfaces, megahertz frequency acoustic waves are substantially attenuated due to the high absorption in air. For these reasons, the performance of air-coupled ultrasound sensing using the traditional piezoelectric and capacitive transducers is severely degraded [6].

Recent advancements in optical-based sensing technologies have opened new possibilities for ultrasound detection [7], [8]. The exceptionally high Q-factors and optomechanical sensitivity of whispering gallery mode (WGM) resonators have been explored for several sensing applications [9]. The interaction of incident acoustic waves with the WGM resonator structure induces structural deformations and/or a change in the refractive index of the glass and, thus, shifts the resonance frequency of the WGM resonator, which can be sensitively monitored. Kim et al. [8] reported on air-coupled capillary-based optical ring resonators achieving a noise equivalent pressure (NEP) as low as 215 and 41 $\text{mPa}/\sqrt{\text{Hz}}$ at 50 and 800 kHz, respectively, and successfully employed these devices for the detection of PA ultrasound pulses. Pan et al. [10] have demonstrated capillary microbubble resonators combined with a digital optical frequency comb readout, reaching an NEP of 4.4 $\text{mPa}/\sqrt{\text{Hz}}$ at 165 kHz. Basiri-Esfahani et al. [11] achieved the NEP of 8–300 $\text{mPa}/\sqrt{\text{Hz}}$ at 1 kHz to 1 MHz using a microdisk resonator. Yang et al. [12] reported an on-chip microtoroid resonator with a sensitivity of 0.046–10 $\text{mPa}/\sqrt{\text{Hz}}$ in a frequency range of 0.25–3.2 MHz.

This work aims to demonstrate an on-chip glass microspherical shell WGM resonator-based air-coupled ultrasound sensor capable of detecting acoustic waves in 0.6–3.5 MHz frequency range with a sensitivity of 40 $\mu\text{Pa}/\sqrt{\text{Hz}}$ at 1.72 MHz. The sensor comprises an on-chip borosilicate glass microspherical shell with a radius of 450 µm and an average shell thickness of 12 µm, which is coupled to a tapered optical fiber to induce optical resonance in the structure. We use a laser Doppler vibrometer (LDV) to directly measure the induced structural deformation in the glass microspherical shell due to incident acoustic waves. A 3D COMSOL finite-element model is used to calculate the axisymmetric vibrational modes of the microspherical shell under a uniform ultrasound force or pressure load conditions. Modal analysis shows good agreement between the finite-element-model-predicted structural resonances of the microspherical shell for the observed structural resonances using WGM measurements. Furthermore, the on-chip microspherical shell WGM resonators can be made completely

Corresponding author: Srinivas Tadigadapa (e-mail: srinivas@northeastern.edu).
Associate Editor: Giacomo Langfelder.
Digital Object Identifier 10.1109/LSENS.2024.3433472

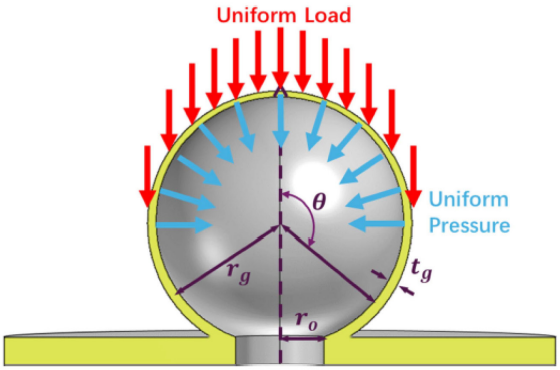

Fig. 1. Schematic of the 3D model showing the uniform force and pressure load boundary conditions used in the FEA simulations.

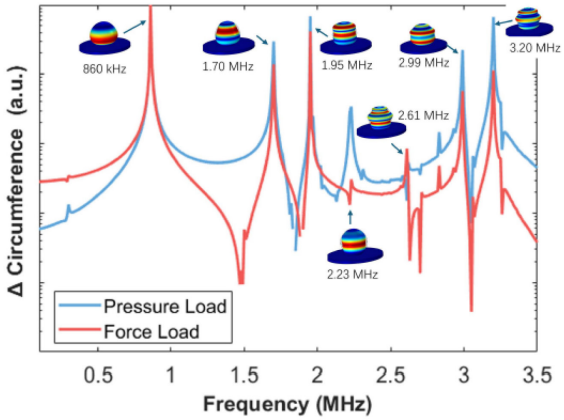

Fig. 2. Change in the microspherical glass shell (radius ~450 μm, average shell thickness of 12 μm) assumed to be rigidly clamped at the bottom of along a circular edge under uniform force (red) and pressure (blue) loads applied only to the top half of the shell (see Fig. 1). Insets show the mode shapes associated with the observed resonance peaks.

transparent in the visible region, which can greatly simplify their integration into PA imaging setups.

II. THEORY, EXPERIMENTS, AND DISCUSSION

A. Analytical Modeling and Finite-Element Analysis

To better predict the performance of glass microspherical shell WGM resonators for high-frequency ultrasound sensing applications, it is critical to understand the natural frequencies and mode shapes of the structural resonances. This knowledge is vital for estimating the dynamic range and sensitivity of the WGM ultrasound sensor. The resonance frequencies f_m of a spherical shell under arbitrary boundary conditions are derived in [13]

$$f_m = \frac{1}{2\pi} \cdot \frac{k_m}{r_g} \cdot \sqrt{\frac{E}{\rho\left(1-\nu^2\right)}} \tag{1}$$

where the material used here was Schott Borofloat 33, characterized by Young's modulus E of 64 GPa, Poisson's ratio ν of 0.2, and a density ρ of 2230 kg/m^3. r_g of 450 µm was used as the radius of microspherical shell. k_m is a dimensionless parameter that depends on the physical parameters of the shell [14]. It was calculated by solving the characteristic equation of the mechanical system for the given boundary conditions. Mode number m is the order of Legendre functions, and the only symmetric mode in the first four modes calculated is when m equals to 0. For mode $m = 0$, the calculated frequency was 1.024 MHz using the aforementioned formula for $k_m = 0.525$. As shown next, this frequency overestimates the first symmetric mode resonance due to the ideal assumption of uniform glass shell thickness. However, the glass blowing process results in nonuniform shell wall thickness; being thinner in the top half of the shell and thicker in the bottom half of the shell and is likely the explanation for this difference.

A 3D finite-element analysis (FEA) model was employed to provide a more accurate cross verification of the symmetric modes. Here, the microspherical shells are assumed to be of nonuniform wall thickness but perfectly spherical and elastic and with the circular edge where it is attached to the substrate to be rigidly clamped. Fig. 1 shows the FEA model used in this letter. $t_g(\theta)$ is the θ-dependent thickness of the glass shell, and r_o is the radius of the etched cavity in the silicon. After estimating the natural frequency via an eigenfrequency analysis, frequency-domain studies were conducted to examine the deformation of the microspherical shell under various loads. The simulations were conducted using the following dimensions of the microshperical shell in this study, r_o= 150 μm, r_g = 450 μm, and $t_g(\theta)$ = 7–15 μm. In these simulations, conducted on the 3D model in COMSOL, two types of loads were applied to only the top half of the sphere: a uniform force in the z-direction and a uniform radially inward pressure load. It was observed that unlike the eigenfrequency analysis, both these types of loads excited only the axisymmetric modes. Fig. 2 shows the simulated change in the equatorial plane circumference of the microspherical shell as a function of the frequency of the applied uniform acoustic pressure and force loads. It was observed that peaks occurred at each axisymmetric mode, with the modes becoming increasingly closely spaced beyond the second order.

B. LDV Measurement

We employed an LDV to measure the minute vibrations and deformations induced in glass microspherical shell by incident acoustic waves. The shell was positioned so that the LDV's laser could directly target the equator of the shell, the point where the optical fiber in the WGM experiments would be coupled. The ultrasound actuator was placed facing the top of the microspherical shell to mimic the boundary conditions used in the COMSOL model. This positioning ensures that the LDV measures the equatorial radial displacement, as modeled by frequency-domain analysis.

Prior to the measurement, the microspherical shell is coated with gold to ensure adequate reflectivity. This coating ensures that the shell surface effectively reflects the laser beam back into the LDV optics, a critical requirement for accurate measurement of vibrations using the LDV. Due to the nonplanarity of the spherical surface of the shell, only a small area on the shell reflects the laser back to provide valid displacement data. The ultrasound transducer, powered by the internal signal generator of the LDV, was placed facing the top of microspherical shell (i.e., parallel to the plane of substrate on which the microspherical shell is blown) and is a single-element device with a resonance frequency at ~5 MHz and is placed at a distance of 1 cm from the top of the microspherical shell. The transducer is considered as a point source that radiates spherical acoustic waves with frequency-dependent attenuation in air [15].

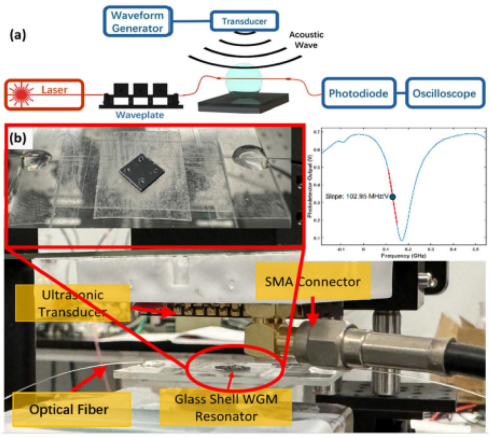

Fig. 3. (a) Schematic of the test setup. (b) Photo of the measurement setup. The WGM resonator is placed at the bottom facing the ultrasound transducer placed ~1 cm above on an XYZ stage and is powered using a waveform generator through the SMA connector. (Inset) Typical resonance curve of the WGM device. *X*-axis represents the frequency sweep of the laser of about 1550 nm. FWHM gives a *Q*-factor of 2×10^6.

A continuous sine wave is used to drive the ultrasound transducer, sweeping frequencies from 0.6 to 3.5 MHz. Fig. 4 shows the LDV measured distortion (displacement) as a function of incident acoustic frequency. This experiment was critical in confirming that the later results obtained using the WGM experiments were indeed induced due to the structural distortions in the equatorial plane of the microspherical shell.

C. WGM Measurement

The experimental setup used to measure the transducer output using the WGM resonator is shown in Fig. 3. A microspherical shell of 450-μm radius is coupled to a tapered optical fiber, one end of which is connected to a tunable laser (1550 nm) to excite resonance in the device and to a photodetector on the other end. The absorption of the wavelengths at the optical resonances is seen as a dip in the output of the photodetector and is recorded using an oscilloscope, as shown in Fig. 3(b) inset. The optical resonance of the WGM resonator has a full width at half maximum (FWHM) of 100 MHz, implying a *Q*-factor of ~2 million. The WGM excitation laser is then set to a frequency at the steepest point, where the slope is 102.95 MHz/V, as shown in Fig. 3(b) inset. The relationship between the microspherical shell radius and WGM resonance frequency is calculated to be 2.32 pm/MHz at the equator based on the geometry of the resonator.

The single-element micromachined ultrasound transducer is placed ~1 cm above the WGM resonator and is powered by a waveform generator through an RF cable and the subminiature connector version A (SMA) connector. The ultrasound transducer is driven using a 5-V amplitude continuous sine wave in the frequency range between 600 kHz and 3.5 MHz. The output of the photodetector is collected and processed using fast Fourier transform (FFT) to acquire the WGM optical resonator response. Fig. 4 shows the frequency response of the WGM resonator overlaid with the LDV measured radial distortion at the equator of the microspherical shell. As compared to the frequency-domain COMSOL predictions, the WGM results show four of the first

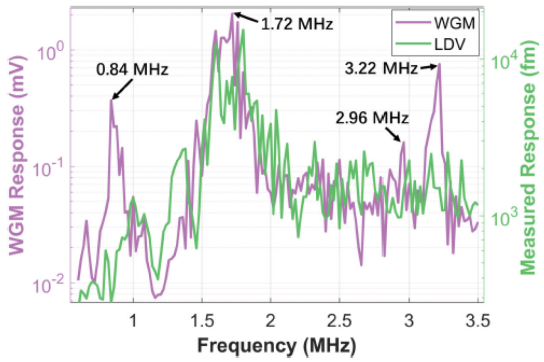

Fig. 4. Frequency response of the WGM resonator. The left axis shows the response of the photodetector when the transducer is driven with a sine signal sweeping from 0.6 to 3.5 MHz. The right axis shows the LDV measured radial distortion at the equator of the microsphere.

seven axisymmetric resonance peaks, and the agreement between the predicted and observed resonances for these peaks is very good. WGM and LDV measurements show a close similarity in their response, especially in the peak between 1.60 and 1.75 MHz, firmly correlating the measured result relationship to the pressure signal impinging on the microspherical shell from the ultrasound transducer. For the LDV measurements, the ultrasound pressure needed for a response to be seen was $\geq$40 times larger than in the WGM experiments. The low overall sensitivity, due to the low level of reflected light reaching its optics from the curved surface of the microspherical shell, made it difficult to observe other resonances in the LDV measurements, while the WGM method is able to resolve additional peaks. It must be noted that for the resonances to be effectively observed by the WGM resonator, the maximum radial distortion has to occur in the plane, where the optical fiber is coupled to the shell. As seen in Fig. 2, not all the mode shapes result in an optimal distortion at the equatorial plane and could easily be missed. For the strongest peak between 1.60 and 1.75 MHz, the maximum radial distortion the WGM measured is ~460 fm and shows both the outstanding sensitivity of the WGM measurement and the challenge of measuring resonances with smaller distortion amplitudes in the equatorial plane.

Both the WGM- and LDV-based measurements show similar broad response peak between 1.6 and 1.75 MHz. This is clearly different from the FEA simulation, in which we have assumed an ideal uniform force/pressure load. We believe that actual pressure/force load from the point source ultrasound transducer is likely to be nonuniform with a complex phase of incidence across the contour of the microspherical shell. Other reflected or diffracted acoustic signals from the substrate and the experimental setup impinging on the microspherical shell could also induce nonaxisymmetric modes of resonance, which if they induce sufficient distortion in the equatorial plane can affect the output. These closely spaced modes in the 1.6–1.75 MHz range and other nonidealities could explain the broad nature of the peak in this frequency range. However, this needs further investigation and is outside the scope of the presented work.

At each ultrasound frequency measured, the magnitude of the WGM resonator's FFT response above the measured noise floor at that frequency is used as the signal strength. The signal-to-noise ratio is then calculated from the measured sensor response and the noise spectrum at each frequency. To experimentally determine the NEP of the sensor, we used the LDV to measure the displacement of

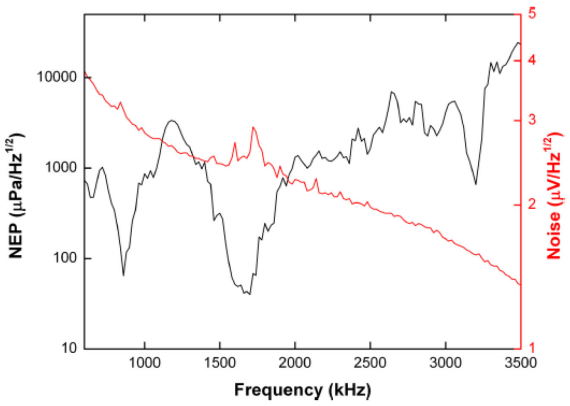

Fig. 5. Calculated NEP of the WGM sensor as a function of ultrasound frequency from 0.6 to 3.5 MHz.

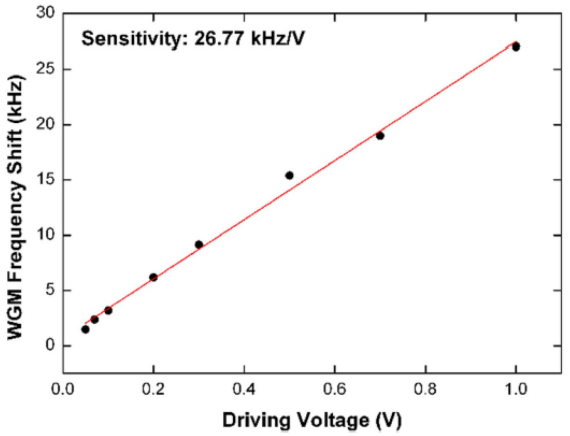

Fig. 6. Linear relationship between WGM resonance frequency shift versus the transducer driving voltage is obtained at 1.65 MHz.

the ultrasound transducer element across different drive frequencies. We then calculated the acoustic pressure produced by the transducer based on the measured displacement, atmospheric attenuation, and the distance to the sensor. The NEP of the WGM resonator for the ultrasound pressure is calculated from these values between 600 kHz and 3.5 MHz and the noise floor measured at each frequency, as shown in Fig. 5. It shows that in this frequency range, the WGM resonator has an NEP between 40 μPa/$\sqrt{}$Hz and 24.2 mPa/$\sqrt{}$Hz, with the best sensitivity achieved at 1.72-MHz ultrasound frequency. A linear relationship between the ultrasound transducer driving voltage and the WGM resonator frequency shift with a slope of 26.77 kHz/V is obtained at 1.65 MHz and is plotted in Fig. 6.

III. CONCLUSION

In conclusion, an on-chip blown glass microspherical shell WGM resonator is demonstrated as a sensitive ultrasound sensor operating in air. An ultrasound NEP of 40 μPa/$\sqrt{}$Hz at 1.72 MHz was obtained using this device. 3D FEA showed a good agreement with the experimentally obtained modal resonances of the microspherical glass shell. The inherent transparency and high ultrasound sensitivity of the glass microspherical shell structure in the visible region make this an attractive sensor for PA sensing and high-frequency air-coupled ultrasound measurements.

ACKNOWLEDGMENT

This work was supported by the National Science Foundation (NSF) under Grant 2053591.

REFERENCES

[1] C. L. Bayer, G. P. Luke, and S. Y. Emelianov, "Photoacoustic imaging for medical diagnostics," *Acoust. Today*, vol. 8, no. 4, pp. 15–23, 2012, doi: 10.1121/1.4788648.
[2] L. V. Wang and S. Hu, "Photoacoustic tomography: In vivo imaging from organelles to organs," *Science*, vol. 335, no. 6075, pp. 1458–1462, 2012.
[3] S. P. Khandare, C. Huang, S. R. Kothapalli, and S. Tadigadapa, "Performance of aluminum nitride curved PMUT arrays fabricated using glass blowing technique," in *Proc. IEEE 37th Int. Conf. Micro Electro Mech. Syst.*, 2024, pp. 198–201, doi: 10.1109/MEMS58180.2024.10439406.
[4] R. E. Green, "Non-contact ultrasonic techniques," *Ultrasonics*, vol. 42, pp. 9–16, 2004, doi: 10.1016/j.ultras.2004.01.101.
[5] G. Rousseau, A. Blouin, and J.-P. Monchalin, "Non-contact photoacoustic tomography and ultrasonography for tissue imaging," *Biomed. Opt. Exp.*, vol. 3, no. 1, pp. 16–25, 2012, doi: 10.1364/BOE.3.000016.
[6] J. R. Lee, N. Sunuwar, and C. Y. Park, "Comparative analysis of laser ultrasonic propagation imaging system with capacitance and piezoelectric air-coupled transducers," *J. Intell. Mater. Syst. Struct.*, vol. 25, pp. 551–562, 2014, doi: 10.1177/1045389X13481253.
[7] G. Wissmeyer, M. A. Pleitez, A. Rosenthal, and V. Ntziachristos, "Looking at sound: Optoacoustics with all-optical ultrasound detection," *Light: Sci. Appl.*, vol. 7, no. 1, 2018, Art. no. 53, doi: 10.1038/s41377-018-0036-7.
[8] K. H. Kim et al., "Air-coupled ultrasound detection using capillary-based optical ring resonators," *Sci. Rep.*, vol. 7, no. 1, 2017, Art. no. 109, doi: 10.1038/s41598-017-00134-7.
[9] C. Zhang, A. Cocking, E. Freeman, Z. Liu, and S. Tadigadapa, "On-chip glass microspherical shell whispering gallery mode resonators," *Sci. Rep.*, vol. 7, no. 1, 2017, Art. no. 14965, doi: 10.1038/s41598-017-14049-w.
[10] J. Pan et al., "Microbubble resonators combined with a digital optical frequency comb for high-precision air-coupled ultrasound detectors," *Photon. Res*, vol. 8, no. 3, 2020, Art. no. 303, doi: 10.1364/prj.376640.
[11] S. Basiri-Esfahani, A. Armin, S. Forstner, and W. P. Bowen, "Precision ultrasound sensing on a chip," *Nature Commun.*, vol. 10, no. 1, 2019, Art. no. 132.
[12] H. Yang et al., "High-sensitivity air-coupled megahertz-frequency ultrasound detection using on-chip microcavities," *Phys. Rev. Appl.*, vol. 18, no. 3, 2022, Art. no. 034035.
[13] F. I. Niordson, "Free vibrations of thin elastic spherical shells," *Int. J. Solids Struct.*, vol. 20, no. 7, pp. 667–687, 1984.
[14] I. P. Prikhodko, S. A. Zotov, A. A. Trusov, and A. M. Shkel, "Microscale glass-blown three-dimensional spherical shell resonators," *J. Microelectromech. Syst.*, vol. 20, no. 3, pp. 691–701, 2011.
[15] C. Huang, S. P. Khandare, S. R. Kothapalli, and S. Tadigadapa, "Characterization of curved piezoelectric micromachined ultrasound transducers fabricated by chip-scale glass blowing technique," *IEEE Sens. Lett.*, vol. 7, no. 10, Oct. 2023, Art. no. 2503304, doi: 10.1109/LSENS.2023.3308112.